Stiffness Evolution in Frozen Sands Subjected to Stress Changes

Sheng Dai, Ph.D., A.M.ASCE[1]; and J. Carlos Santamarina, Ph.D., A.M.ASCE[2]

Abstract: Sampling affects all soils, including frozen soils and hydrate-bearing sediments. The authors monitor the stiffness evolution of frozen sands subjected to various temperature and stress conditions using an oedometer cell instrumented with P-wave transducers. Experimental results show the stress-dependent stiffness of freshly remolded sands, the dominant stiffening effect of ice, creep after unloading, and the associated exponential decrease in stiffness with time. The characteristic time for stiffness loss during creep is of the order of tens of minutes; therefore it is inevitable that frozen soils experience sampling disturbances attributable to unloading. Slow unloading minimizes stiffness loss; conversely, fast unloading causes a pronounced reduction in stiffness probably attributable to the brittle failure of ice or ice-mineral bonding. **DOI:** 10.1061/(ASCE)GT.1943-5606.0001713. © *2017 American Society of Civil Engineers.*

Author keywords: Wave velocity; Sampling effect; Creep; Coda wave interferometry; Cementation; Freeze sampling.

Introduction

Most natural soils experience some degree of bonding or cementation attributable to diagenesis, salt precipitation, bacterial activity, or ice/hydrate formation. The effect of cementation on soil behavior depends on (1) the amount, type, and spatial distribution of the cementing agent; (2) the grain shape, size distribution, and packing density of the host sediment; and (3) the state of stress and stress-cementation histories (Clough et al. 1981; Consoli et al. 2010; Fernandez and Santamarina 2001; Ismail et al. 2002; Khan et al. 2006). Bonding and cementation usually produce a marked increase in stiffness, affect the elastic and volumetric threshold strains, promote dilation during shear, increase drained and undrained strengths, decrease permeability, and hinder liquefaction (Acar and El-Tahir 1986; Baig et al. 1997; DeJong et al. 2006; Dutton and Timothy 1992; Lee et al. 2009; Olague Caballero 2008; Pestana and Salvati 2006; Wang and Leung 2008; Yun and Santamarina 2005). Sampling inevitably induces stresses and strains that may cause soil fabric change by breaking the bonding or cementation. Consequently, postsampling stiffness measurements often show significant differences from field measurements (Rinaldi and Santamarina 2008; Stokoe and Santamarina 2000; Tatsuoka and Shibuya 1991).

The sampling disturbance to frozen soils results from unavoidable stress and thermal changes (Brockett and Lawson 1985; Lange 1968; Zacny and Cooper 2005). Strain rate, temperature, and either tensile or compressive stress change alter the ductile-brittle behavior of ice (Hallett and Newson 2001; Schulson 1999; Schulson and Duval 2009). The mechanical response of frozen sands is affected by temperature (Mühll et al. 2003; Springman et al. 2012; Yamamoto and Springman 2014), the magnitude of the stress change (Alkire and Andersland 1973; Andersland and AlNouri 1970; Domaschuk et al. 1985; Yang et al. 2010), ice content (Arenson et al. 2004; Arenson and Springman 2005; Kurfurst and Pullan 1985), and the specimen's shape and size (Currier and Schulson 1982; Ladanyi and Arteau 1979).

This study explores the change in P-wave velocity in sands during loading, freezing, unloading, ice creep, and ice-melting processes and investigates the effect of loading and unloading rates on the stiffness of frozen sands. Results apply to sampling and aging effects in freeze sampling of unsaturated sands (e.g., to avoid dilation effects in freeze sampling), frozen ground sampling, and core recovery from hydrate-bearing sediments (with hydrate saturations within the range explored in this study).

Experimental Study

The authors subjected unsaturated fine-grained sands to various stress-freezing histories under a zero-lateral-strain boundary condition in an oedometer cell. The following sections describe the experimental device, materials, and test procedures.

Experimental Device

The oedometer cell (inside diameter $d_{in} = 69.8$ mm, height $H = 76.2$ mm) sits within a spring-loaded reaction frame (long spring, initial length $= 152.4$ mm, stiffness $K = 306$ N/mm) to impose a steady vertical stress during loading, freezing, unloading, creep, and melting stages. Piezopads mounted on the top and bottom caps of the oedometer cell measure the vertically propagating P waves. A K-type thermocouple (precision of 0.1°C) detects the temperature at the center of the specimen. The device and sensors are placed inside a freezer set at −10°C. Fig. 1 shows a schematic configuration of the device and sensors.

Specimen Preparation

Specimens were made of fine-grained, uniform, quartzitic sands (Ottawa F110, specific gravity $G_s = 2.65$, mean grain size $D_{50} = 0.12$ mm, maximum and minimum void ratios $e_{max} = 0.848$ and $e_{min} = 0.535$, initial porosity $n = 0.45$, corresponding initial void

---

[1]Assistant Professor, School of Civil and Environmental Engineering, Georgia Institute of Technology, 790 Atlantic Dr., Atlanta, GA 30332-0355 (corresponding author). E-mail: sheng.dai@ce.gatech.edu

[2]Professor, Earth Science and Engineering, King Abdullah Univ. of Science and Technology, Bldg. 5, Room 3218, KAUST, Thuwal 23955-6900, Saudi Arabia. E-mail: carlos.santamarina@kaust.edu.sa

© ASCE   04017042-1   J. Geotech. Geoenviron. Eng.

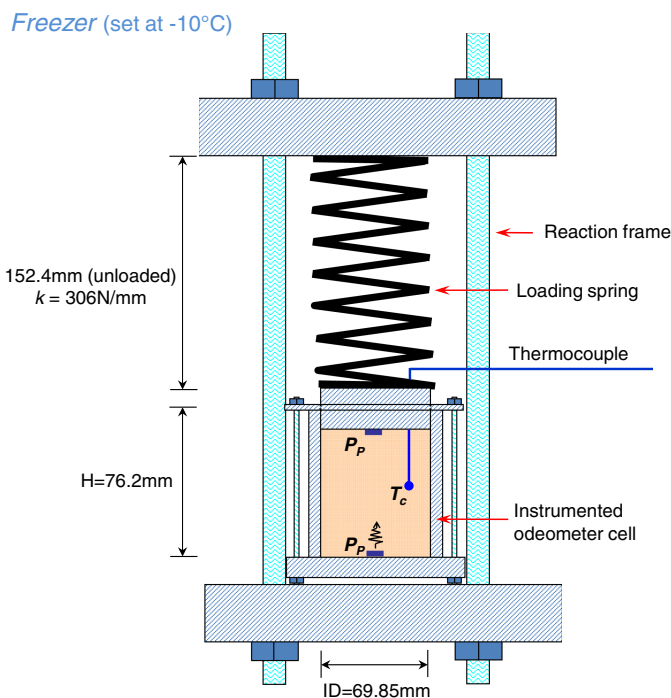J. Geotech. Geoenviron. Eng., 2017, 143(9): 04017042

Fig. 1. Experimental configuration: an oedometer cell equipped with piezopads (P_P) and a thermocouple (T_c) sits within a spring-loaded reaction frame in a freezer

Fig. 2. Cascade of selected P-wave signatures gathered during various experimental stages (specimen: initial water content % by weight = 5)

ratio $e_0 = 0.82$, coefficient of uniformity $C_u = 1.7$, coefficient of curvature $C_c = 0.99$, roundness $R = 0.7$, and sphericity $S = 0.7$). The sands were homogeneously mixed with a predetermined amount of water to attain a target water content (2, 5, 10, and 20% by weight). Finally, the homogeneously mixed, partially saturated sands were scooped into the oedometer cell and uniformly tamped.

Experimental Procedure

Each specimen experienced five successive stress-temperature stages: (1) loading from $\sigma_v = 1$ to 600 kPa at constant room temperature $T = 20$°C; (2) cooling from 20 to -10°C to cause ice formation at constant applied vertical stress $\sigma_v = 600$ kPa for 24 h; (3) vertical stress relaxation from 600 to 1 kPa at constant temperature $T = -10$°C; (4) creep at constant vertical stress $\sigma_v = 1$ kPa and temperature $T = -10$°C; and finally (5) heating from $T = -10$°C to room temperature $T = 20$°C at constant vertical stress $\sigma_v = 1$ kPa. P-wave signals were recorded throughout all stages.

The ice saturations $S_{ice} = V_{ice}/V_{void}$ at the end of Step 2 were $S_{ice} = 0.06, 0.15, 0.30$, and 0.52 for the different initial water saturations: 2, 5, 10, and 20% by weight. (Estimated ice saturations reflect initial porosity and water content and take into consideration the water-to-ice volume expansion.) Water forms menisci at interparticle contacts in specimens with low water saturation and converts into ice at contacts after freezing. Some water migration toward the boundary is anticipated in the specimen with 20% water by weight because of cryogenic suction during freezing.

P-Wave Signatures Analysis

Fig. 2 presents a subset of P-wave signatures gathered during the various experimental stages. Time shifts in the first arrivals during the loading, freezing, and thawing stages can be easily distinguished. However, changes in signatures in frozen sand during unloading and subsequent creep stages are almost indiscernible.
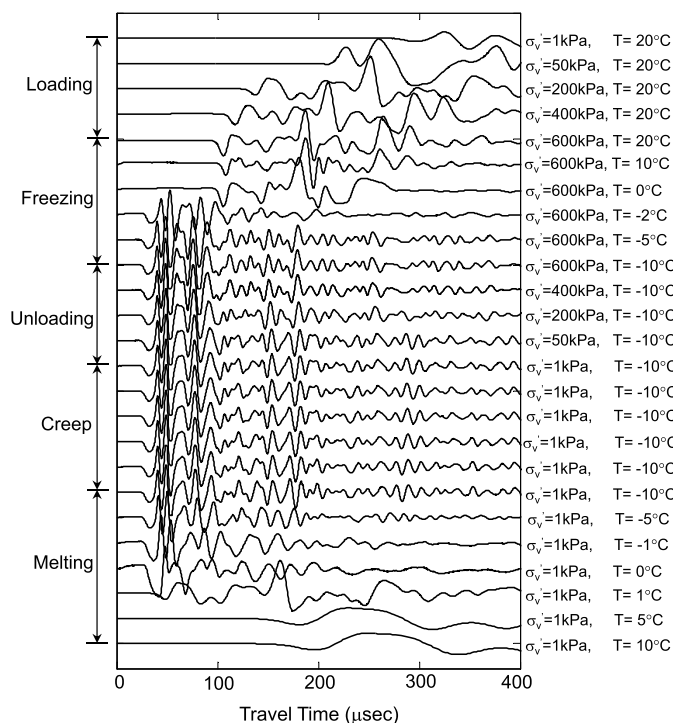
The first arrival reflects the fastest wave propagation path between the source and the receiver; later, coda wave arrivals correspond to longer wave travel paths after multiple internal reflections (Snieder et al. 2002). Minute time shifts between any two consecutive signals become gradually more pronounced in these late arrivals, as illustrated in Fig. 3; in fact, time shifts increase almost linearly with the travel time for these longer wave paths recorded in the signal coda. Thus, one can time-stretch one signal relative to the other until their cross-correlation is maximized; then, the stretching
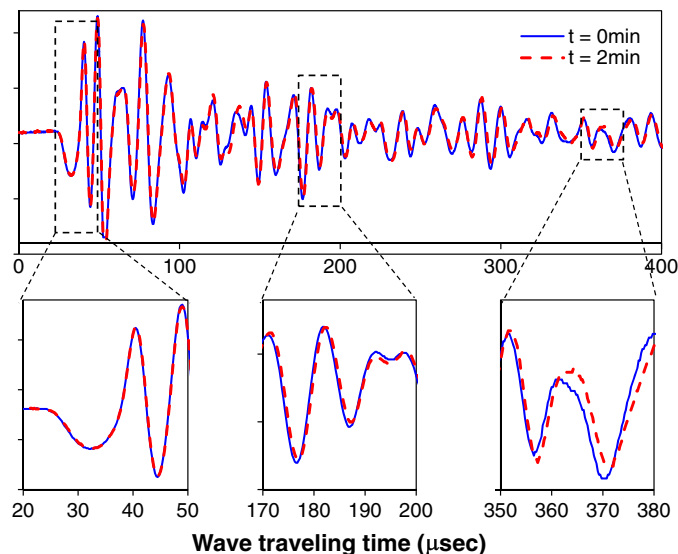

Fig. 3. Coda wave analysis; illustration using two consecutive P-wave signatures gathered for the specimen with ice saturation $S_{ice} = 0.06$ during the creep stage; while there is no measurable difference in the first arrivals, wave codas can be used to detect minute velocity changes
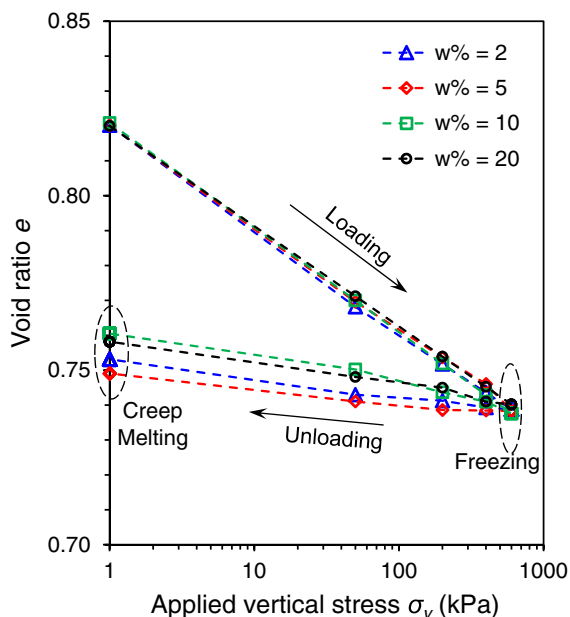
© ASCE 04017042-2 J. Geotech. Geoenviron. Eng.

J. Geotech. Geoenviron. Eng., 2017, 143(9): 04017042

Fig. 4. Evolution of void ratio throughout the experiments; marked volume changes are caused by loading and unloading; freezing, creep, and melting result in undiscernible volumetric changes in this study

factor is used to compute the change in travel time for the first arrival [details and limitations of coda wave analysis can be found in Dai et al. (2013) and Wuttke et al. (2012)].

Experimental Results

Volumetric Change

The evolution of void ratio during each experimental stage for all specimens is shown in Fig. 4. Most volumetric changes occurred during the loading and unloading stages, and there was no discernable change in void ratio during the freezing, creep, and melting stages. All specimens started with an initial void ratio of $e_0 = $ ~0.82 and reached final void ratios of $e_f = $ ~0.75–0.76 at the end of the test.

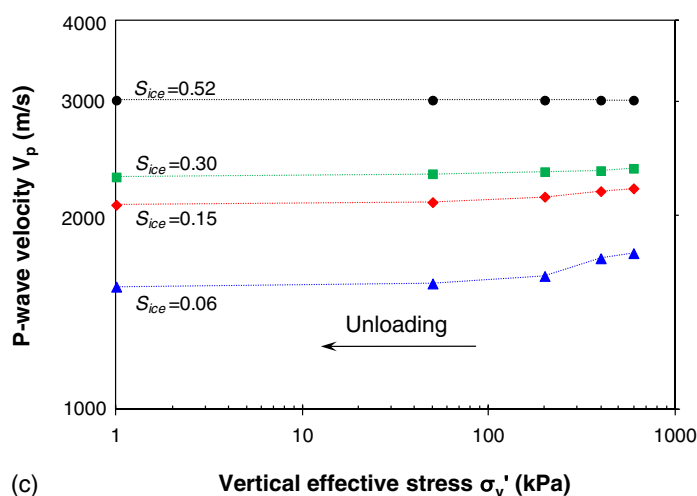### P-Wave Velocity Evolution during Loading (Unfrozen at Room Temperature)

P-wave velocities during loading at constant room temperature were very similar for all specimens [Fig. 5(a), $T = 20°C$]. The P-wave velocity increases with the applied vertical stress following a power Hertzian-like response, i.e., a linear trend in a log-log scale. Deviation from linearity at low stresses <10 kPa reflects the role of
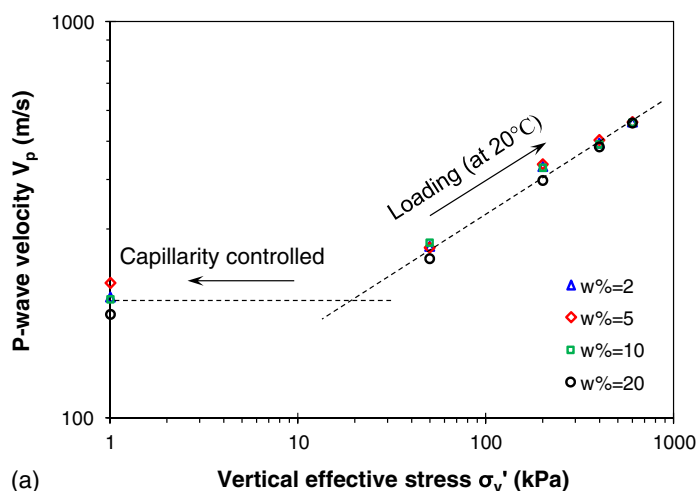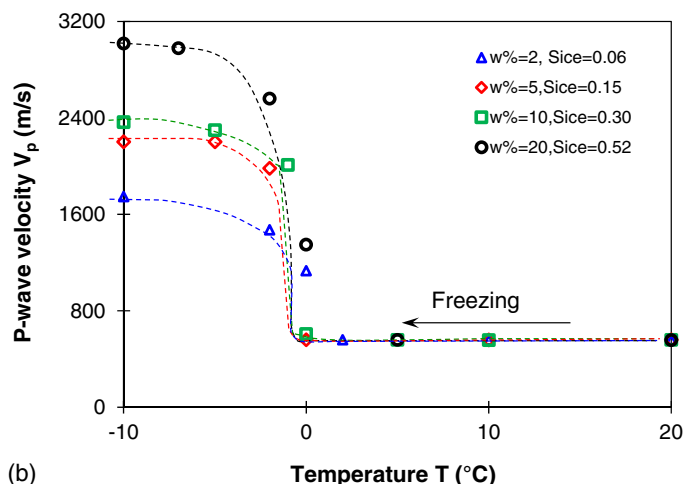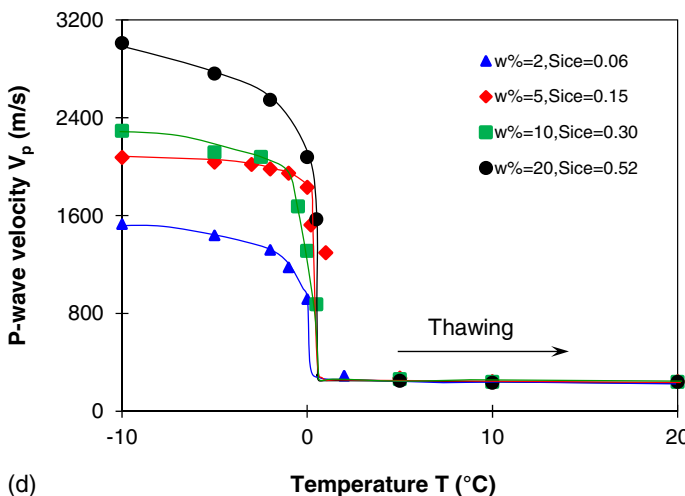
Fig. 5. Evolution of the P-wave velocity during each experimental stage: (a) loading at temperature $T = 20°C$; (b) freezing at constant applied vertical stress $\sigma_v = 600$ kPa; (c) unloading at temperature $T = -10°C$; (d) thawing at constant stress $\sigma_v = 1$ kPa

© ASCE   04017042-3   J. Geotech. Geoenviron. Eng.

J. Geotech. Geoenviron. Eng., 2017, 143(9): 04017042

capillarity on the skeleton stiffness; notably, the P-wave velocity at very low stress ($\sigma_v = 1$ kPa) slightly increases with the decreasing water content.

P-Wave Velocity Evolution during Freezing (at Constant Vertical Stress)

Fig. 5(b) shows the evolution of P-wave velocity during freezing at constant vertical stress $\sigma_v = 600$ kPa for the four specimens. There is a decisive increase in velocity when the temperature measured at the center of the specimens approaches the freezing point ($T = 0°C$). The P wave reaches the maximum value when all free water freezes. The final velocity increases with ice content S_{ice}.

P-Wave Velocity Evolution during Unloading (Frozen at Constant Temperature $-10°C$)

In order to study stiffness loss in frozen soils during unloading and relaxation, the authors decreased the applied vertical stress from $\sigma_v = 600$ to 1 kPa at a constant temperature $T = -10°C$.

Unloading takes place in four stages, holding each load for 10 min. No specimen experiences more than 10% velocity loss during unloading. Specimens with higher ice saturation exhibit a lower stiffness loss. Fig. 5(c) presents the change in P-wave velocity during unloading.

Creep of Frozen Sands after Unloading (Frozen at Constant Stress and Temperature)

P-wave velocities were monitored for 2 h after the final unloading to a nominal stress $\sigma_v = 1$ kPa and at constant temperature $T = -10°C$. Measured P-wave velocities show that stiffness decays exponentially with time in all tested specimens during the creep stage [Fig. 6(a)].

P-Wave Velocity Evolution during Thawing (Constant Stress)

Specimens were warmed to room temperature $T = 20°C$ at the end of the test. The velocity evolution during thawing is the opposite of
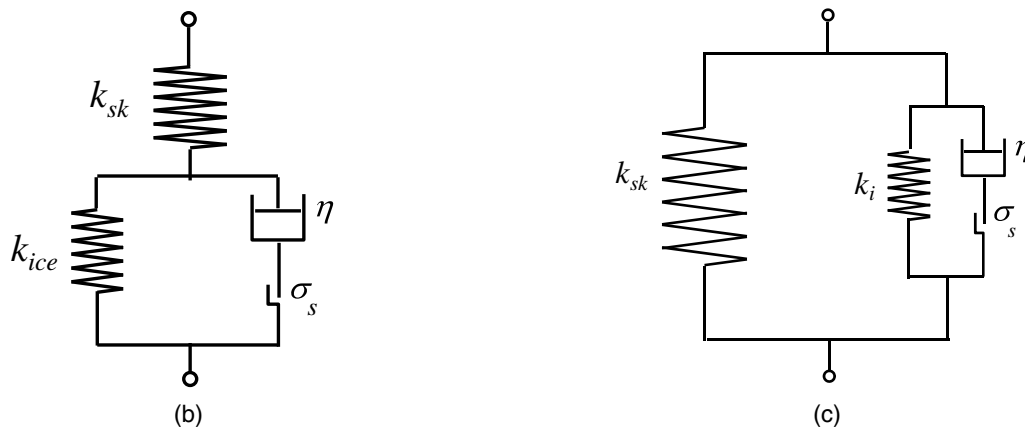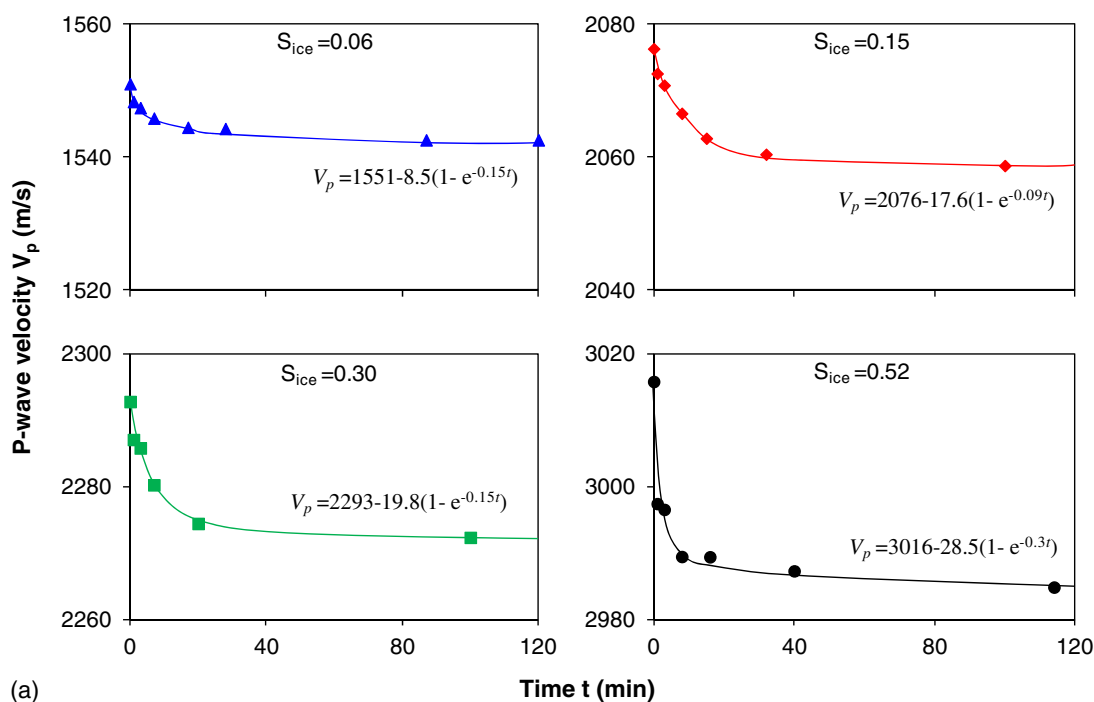
Fig. 6. Evolution of P-wave velocity during creep: (a) P-wave velocities for specimens with different ice saturations during creep following unloading from $\sigma_v = 50$ to 1 kPa at constant temperature $T = -10°C$; dots represent experimental results and lines are the fitted model; conceptual viscoelastoplastic models for a lumped frozen soil mass; (b) ice-free sands in series with frozen sands; (c) ice-free sands in parallel with frozen sands

the evolution during freezing [Fig. 5(d)]. The highest loss in stiffness occurs when the temperature measured at the center of the specimen approaches the melting point $T = 0°C$ [see similar stiffness-temperature response trends in Andersland and Ladanyi (2004)]. The final velocity at room temperature $T = 20°C$ and $\sigma_v = 1$ kPa is approximately 20% higher than the initial velocity at $\sigma_v = 1$ kPa before freezing. This higher remnant stiffness reflects the residual effects that the loading-freezing history left on the particle contacts and the fabric.

Analyses and Discussion

Velocity Loss during Creep after Unloading

The decrease in P-wave velocity with time V_t in the frozen sand specimens after unloading follows an exponential trend [Fig. 6(a)]

$$V_t = V_0 - \Delta V(1 - e^{-\alpha t}) \quad (1)$$

where V_0 = initial velocity before unloading; ΔV = total velocity loss at infinite time; and the α constant captures the characteristic time $1/\alpha$ for velocity decrease, i.e., when 63.2% of the velocity loss has already taken place. The characteristic time for velocity loss during the creep stage is just a few minutes for all specimens tested in this study. This short period suggests that unloading-induced sampling effects are inevitable as specimens cannot be recovered and reloaded fast enough in most onshore and offshore situations. The total velocity loss ΔV attributable to an unloading of 50-kPa vertical stress is relatively small and is approximately 1% of the initial velocity V_0 for all tested specimens, regardless of ice saturation.

Rate of Unloading

Grains tend to rebound during unloading and cause tensile strain in the ice mass that formed while the sand skeleton experienced high confining stress. The mineral-ice-mineral system can break either by (1) ice tensile failure when the mineral is hydrophilic [tensile strength ~2.3 MPa (Petrovic 2003)] or (2) ice-mineral debonding, typically when the mineral is hydrophobic (Jung and Santamarina 2011). A lumped parameter model of the frozen soil mass [Fig. 6(b)] involves an elastic model for the soil skeleton (k_{sk}) and a viscoelastoplastic model for ice ($k_{ice} - \eta - \sigma_s$), where k_{ice} is the elasticity modulus of a Hookean spring element, η is the viscosity parameter of a nonlinear dashpot element, and σ_s is the yield stress of a sliding frictional element. Taking the conceptual model of ice-free sands in series with ice-bonded sands as an example [Fig. 6(b), left illustration], the lumped stiffness of the frozen soil mass subjected to an external stress σ_{ext} lower than σ_s (i.e., without breaking the ice-mineral bond) is

$$k_{lumped} = \frac{\sigma_{ext}}{\frac{\sigma_{ext}}{k_{sk}} + \frac{\sigma_{ext}}{k_{ice}}(1 - e^{-k_{ice}t/\eta})} = \frac{1}{1/k_{sk} + (1 - e^{-k_{ice}t/\eta})/k_{ice}} \quad (2)$$

Thus, k_{lumped} decreases from k_{ek} at $t = 0$ exponentially down to $k_{sk}k_{ice}/(k_{sk} + k_{ice})$ at $t = \infty$

$$\varepsilon_{ice} = \frac{\sigma_{ice}}{k_{ice}}\left[1 - \exp\left(-\frac{k_{ice}}{\eta}t\right)\right] = \frac{\sigma_{ice}}{k_{ice}}[1 - \exp(-\alpha t)] \quad (3)$$

$$\sigma_{ext} = \sigma_{sk(t)} + \sigma_{ice(t)}nS_{ice} \quad (4)$$

$$\varepsilon_{ice(t)} = \frac{\sigma_{ext}[1 - \exp(-\alpha t)]}{nS_{ice}k_{ice} + k_{sk}[1 - \exp(-\alpha t)]} \quad (5)$$

where σ_{ice} = stress applied on the ice. Consequently, sampling effects in frozen ground are stress-rate dependent: frozen sands that are unloaded faster than the ice creep rate ($\dot{\varepsilon}_{ice} \gg \sigma_{ice}/\eta$) can experience ice tensile failure or debonding; by contrast, slow unloading (e.g., $\dot{\varepsilon}_{ice} \ll \sigma_{ice}/\eta$) allows ice creep and preserves the bonded fabric.

The authors conducted additional experiments to corroborate the effect of unloading rate on the stiffness changes in frozen sands. Two specimens with the same ice saturation ($S_{ice} = 0.05$) were kept under a constant stress $\sigma_v = 600$ kPa and temperature $T = -10°C$ for 24 h. The two specimens were then (1) unloaded from 600 kPa down to 1 kPa over different times, one in 2 min to simulate fast unloading and the other in 1 h to simulate slow unloading; (2) allowed to creep for 2 h; and (3) reloaded back to 600 kPa within 2 min. The authors repeated the same three-stage procedure for another two specimens with a higher ice saturation, $S_{ice} = 0.30$. Fig. 7(a) presents a summary of P-wave velocities measured during
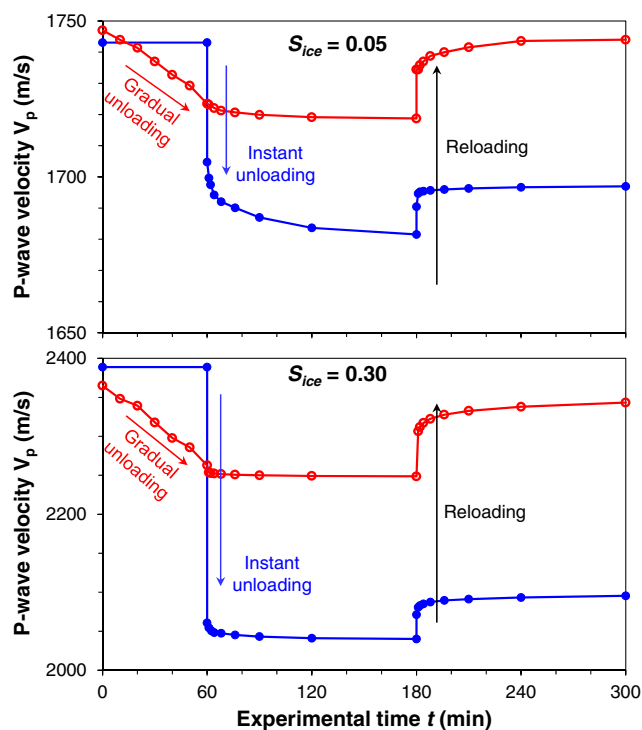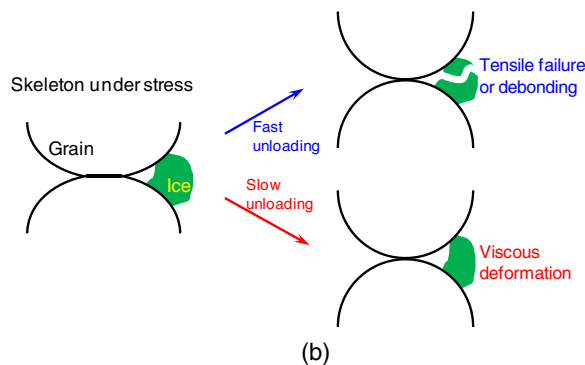
Fig. 7. Effect of unloading rates on the stiffness of partially frozen sands: (a) evolution of P-wave velocities for sands with different ice saturations S_{ice} during unloading (from $\sigma_v = 600$ to 1 kPa) and reloading (from $\sigma_v = 1$ to 600 kPa); (b) schematic illustration of the effect of unloading rates on ice bonding
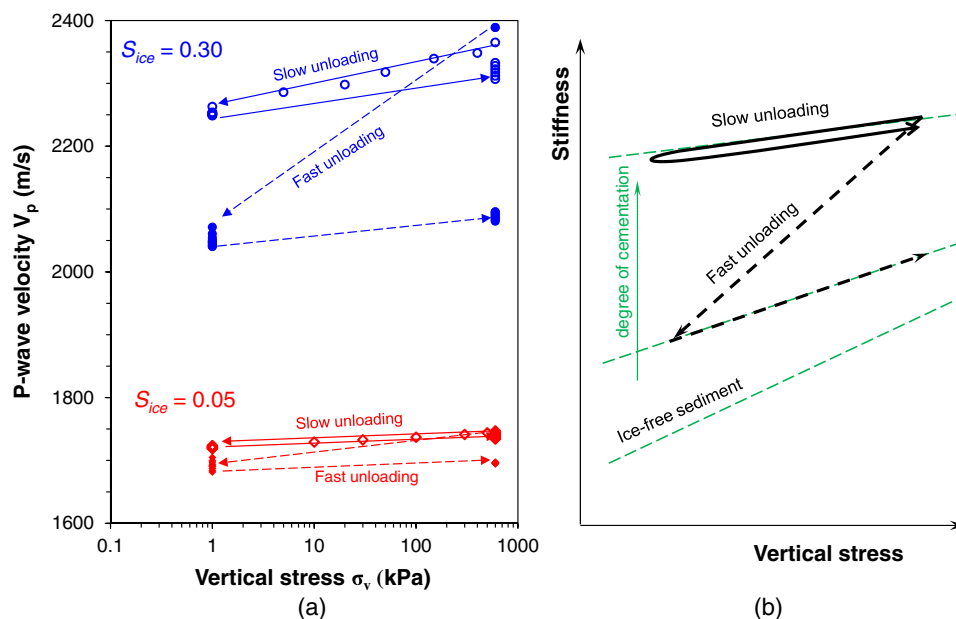
© ASCE

04017042-5

J. Geotech. Geoenviron. Eng.

Fig. 8. Effects of stress-change rates on the stiffness of partially frozen soils during unloading: (a) experimental data for specimen with $S_{ice} = 0.05$ and 0.30; (b) illustration of stiffness evolution during unloading: fast unloading breaks bonds; the specimen stiffness follows the trend for specimens with a lower degree of bonding during reloading; slow unloading allows for creep and preserves the bonding effect of ice

all experimental stages. Results show that fast unloading causes a higher velocity loss than slow unloading, and specimens that experience fast unloading do not fully recover their initial stiffness after reloading, probably because of permanent ice failure or ice-mineral debonding; by contrast, specimens subjected to slow unloading recover most of their initial stiffness [see also Fig. 7(b)].

Stress-Freeze-Creep History

Grain-scale analyses suggest that load-freeze and freeze-load formation histories lead to similar frozen soil stiffness (Fernandez and Santamarina 2001; Rinaldi and Santamarina 2008). Ice creeps and transfers its stress to the granular skeleton during either load-freeze-creep or freeze-load-creep histories. Then, regardless of the formation history, sudden unloading may result in stiffness loss attributable to the tensile failure of ice or ice-mineral debonding when the mineral skeleton rebounds after unloading, as shown in Fig. 8.

Extension to Natural Systems

Ice and hydrates provide structural stability to sands; this resembles the enhanced stability of diagenetically modified sands (either bio-mediated or abiotic). The stiffness-stress response for all cemented soils follows similar patterns: stiffness is controlled by cementation at low stress (even in the case of light cementation); yet, stress eventually determines stiffness at high stress levels. The role of cementation on stiffness is particularly effective when cement formation or precipitation takes place at interparticle contacts, such as the freezing of unsaturated soils in this study.

Cementation locks in porosity and hinders compaction during subsequent sedimentation. Consequently, cementation loss such as ice melting in permafrost or carbonate dissolution attributable to groundwater acidification may trigger volume collapse and instability in sediments that experienced cementation before loading. This situation may develop in a wide range of conditions, from hydrate-bearing permafrost sands, e.g., Mount Elbert, Alaska North Slope (Dai et al. 2011), to reactive fly ash in storage ponds.

Conclusions

Ice (or hydrate) content and its distribution in pores dominate the stiffness of frozen ground (and hydrate-bearing sediments) at low stress. Notably, the role of ice (or hydrate) on stiffness is most pronounced when it forms at interparticle contacts. Other factors include the rate of stress change compared to the ice (or hydrate) creep rate.

Sampling-induced stress and temperature changes can cause a pronounced decrease in stiffness in frozen sands and hydrate-bearing sands. The P-wave velocity decreases exponentially with time after unloading, and the characteristic time is of the order of minutes. Therefore, sampling effects are inevitable as specimens cannot be recovered and reloaded fast enough in both onshore and offshore situations.

The mechanical response of frozen sands is stress-rate dependent. Unloading faster than the ice creep rate can cause ice tensile failure or debonding; slow unloading allows ice to creep and the fabric is better preserved. Even when the in situ state of stress is restored, specimens that experienced fast unloading do not fully recover their initial stiffness within the short laboratory time scales. Conversely, specimens subjected to slow unloading recover most of their initial stiffness after reloading.

Acknowledgments

References

Acar, Y. B., and El-Tahir, E.-T. A. (1986). "Low strain dynamic properties of artificially cemented sand." *J. Geotech. Eng.*, 10.1061/(ASCE)0733-9410(1986)112:11(1001), 1001–1015.

© ASCE   04017042-6   J. Geotech. Geoenviron. Eng.

J. Geotech. Geoenviron. Eng., 2017, 143(9): 04017042

Alkire, B. D., and Andersland, O. B. (1973). "The effect of confining pressure on the mechanical properties of sand-ice materials." *J. Glaciol.*, 12(66), 469–481.

Andersland, O. B., and AlNouri, I. (1970). "Time-dependent strength behavior of frozen soils." *J. Soil Mech. Found. Div.*, 96(4), 1249–1265.

Andersland, O. B., and Ladanyi, B. (2004). *Frozen ground engineering*, Wiley, New York.

Arenson, L. U., Johansen, M. M., and Springman, S. M. (2004). "Effects of volumetric ice content and strain rate on shear strength under triaxial conditions for frozen soil samples." *Permafrost Periglacial Processes*, 15(3), 261–271.

Arenson, L. U., and Springman, S. M. (2005). "Triaxial constant stress and constant strain rate tests on ice-rich permafrost samples." *Can. Geotech. J.*, 42(2), 412–430.

Baig, S., Picornell, M., and Nazarian, S. (1997). "Low strain shear moduli of cemented sands." *J. Geotech. Geoenviron. Eng.*, 10.1061/(ASCE)1090-0241(1997)123:6(540), 540–545.

Brockett, B. E., and Lawson, D. E. (1985). "Prototype drill for core sampling fine-grained perennially frozen ground." *DTIC Document*, Cold Regions Research and Engineering Laboratory, Hanover, NH.

Clough, G. W., Rad, N. S., Bachus, R. C., and Sitar, N. (1981). "Cemented sands under static loading." *J. Geotech. Eng. Div.*, 107(6), 799–817.

Consoli, N. C., Cruz, R. C., Floss, M. F., and Festugato, L. (2010). "Parameters controlling tensile and compressive strength of artificially cemented sand." *J. Geotech. Geoenviron. Eng.*, 10.1061/(ASCE)GT.1943-5606.0000278, 759–763.

Currier, J. H., and Schulson, E. M. (1982). "The tensile strength of ice as a function of grain size." *Acta Metall.*, 30(8), 1511–1514.

Dai, S., Lee, C., and Carlos Santamarina, J. (2011). "Formation history and physical properties of sediments from the Mount Elbert Gas Hydrate Stratigraphic Test Well, Alaska North Slope." *Mar. Pet. Geol.*, 28(2), 427–438.

Dai, S., Wuttke, F., and Santamarina, J. C. (2013). "Coda wave analysis to monitor processes in soils." *J. Geotech. Geoenviron. Eng.*, 10.1061/(ASCE)GT.1943-5606.0000872, 1504–1511.

DeJong, J. T., Fritzges, M. B., and Nüsslein, K. (2006). "Microbially induced cementation to control sand response to undrained shear." *J. Geotech. Geoenviron. Eng.*, 10.1061/(ASCE)1090-0241(2006)132:11(1381), 1381–1392.

Domaschuk, L., Knutsson, S., Shields, D. H., and Rahman, M. G. (1985). "Creep of frozen sand under isotropic and deviatoric components of stress." *J. Energy Res. Technol.*, 107(2), 199–203.

Dutton, S. P. D., and Timothy, N. (1992). "Evolution of porosity and permeability in the lower Cretaceous Travis peak formation, east Texas." *AAPG Bull.*, 76(2), 252–269.

Fernandez, A. L., and Santamarina, J. C. (2001). "Effect of cementation on the small-strain parameters of sands." *Can. Geotech. J.*, 38(1), 191–199.

Hallett, P., and Newson, T. (2001). "A simple fracture mechanics approach for assessing ductile crack growth in soil." *Soil Sci. Soc. Am. J.*, 65(4), 1083–1088.

Ismail, M. A., Joer, H. A., Sim, W. H., and Randolph, M. F. (2002). "Effect of cement type on shear behavior of cemented calcareous soil." *J. Geotech. Geoenviron. Eng.*, 10.1061/(ASCE)1090-0241(2002)128:6(520), 520–529.

Jung, J. W., and Santamarina, J. C. (2011). "Hydrate adhesive and tensile strengths." *Geochem. Geophys. Geosyst.*, 12(8), 1–9.

Khan, Z., Majid, A., Cascante, G., Hutchinson, D. J., and Pezeshkpour, P. (2006). "Characterization of a cemented sand with the pulse-velocity method." *Can. Geotech. J.*, 43(3), 294–309.

Kurfurst, P. J., and Pullan, S. (1985). *Field and laboratory measurements of seismic and mechanical properties of frozen ground*, A.A. Balkema, Rotterdam, Netherlands, 255–262.

Ladanyi, B., and Arteau, J. (1979). "Effect of specimen shape on creep response of a frozen sand." *Eng. Geol.*, 13(1–4), 207–222.

Lange, G. R. (1968). "Rotary drilling and coring in permafrost. Part I: Preliminary investigation, Fort Churchill, Manitoba." *DTIC Document*, Defense Technical Information Center, Fort Belvoir, VA.

Lee, M.-J., Choi, S.-K., and Lee, W. (2009). "Shear strength of artificially cemented sands." *Mar. Georesour. Geotechnol.*, 27(3), 201–216.

Mühll, D. V., Arenson, L., and Springman, S. (2003). "Temperature conditions in two Alpine rock glaciers." *Proc., 8th Int. Conf. on Permafrost*, Swets & Zeitlinger, Lisse, Netherlands, 1195–1200.

Olague Caballero, R. I. (2008). "Oedometric and shearing response of naturally cemented sands of southern New Mexico." Ph.D. dissertation, New Mexico State Univ., Las Cruces, NM.

Pestana, J. M., and Salvati, L. A. (2006). "Small-strain behavior of granular soils. I: Model for cemented and uncemented sands and gravels." *J. Geotech. Geoenviron. Eng.*, 10.1061/(ASCE)1090-0241(2006)132:8(1071), 1071–1081.

Petrovic, J. J. (2003). "Review mechanical properties of ice and snow." *J. Mater. Sci.*, 38(1), 1–6.

Rinaldi, V. A., and Santamarina, J. C. (2008). "Cemented soils: Small strain stiffness." *Deformation characteristics of geomaterials*, IOS Press, Netherlands, 267–273.

Schulson, E. M. (1999). "The structure and mechanical behavior of ice." *JOM*, 51(2), 21–27.

Schulson, E. M., and Duval, P. (2009). *Creep and fracture of ice*, Cambridge University Press, Cambridge, U.K.

Snieder, R., Grêt, A., Douma, H., and Scales, J. (2002). "Coda wave interferometry for estimating nonlinear behavior in seismic velocity." *Science*, 295(5563), 2253–2255.

Springman, S. M., et al. (2012). "Multidisciplinary investigations on three rock glaciers in the Swiss Alps: Legacies and future perspectives." *Geografiska Annaler: Ser. A, Phys. Geogr.*, 94(2), 215–243.

Stokoe, K. H., and Santamarina, J. (2000). "Seismic-wave-based testing in geotechnical engineering." *Int. Conf. on Geotechnical and Geological Engineering, GeoEng 2000*, International Society for Rock Mechanics, Lisboa, Portugal, 1490–1536.

Tatsuoka, F., and Shibuya, S. (1991). "Deformation characteristics of soils and rocks from field and laboratory tests." *Proc., 9th Regional Conf. on Soil Mechanics and Foundation Engineering, Organizing Committee for the Asian Regional Conf. on Soil Mechanics and Foundation Engineering*, Singapore, 101–170.

Wang, Y.-H., and Leung, S.-C. (2008). "A particulate-scale investigation of cemented sand behavior." *Can. Geotech. J.*, 45(1), 29–44.

Wuttke, F., Asslan, M., and Schanz, T. (2012). "Time-lapse monitoring of fabric changes in granular materials by coda wave interferometry." *ASTM Geotech. Test. J.*, 35(2), 353–362.

Yamamoto, Y., and Springman, S. M. (2014). "Axial compression stress path tests on artificial frozen soil samples in a triaxial device at temperatures just below 0°C." *Can. Geotech. J.*, 51(10), 1178–1195.

Yang, Y., Lai, Y., and Chang, X. (2010). "Experimental and theoretical studies on the creep behavior of warm ice-rich frozen sand." *Cold Reg. Sci. Technol.*, 63(1–2), 61–67.

Yun, T. S., and Santamarina, J. C. (2005). "Decementation, softening, and collapse: Changes in small-strain shear stiffness in k0 loading." *J. Geotech. Geoenviron. Eng.*, 10.1061/(ASCE)1090-0241(2005)131:3(350), 350–358.

Zacny, K. A., and Cooper, G. A. (2005). "Investigation of the performance of a coring bit in frozen mud under Martian conditions of low temperature and pressure." *J. Geophys. Res. Part E Planets*, 110(4), 8.

© ASCE 04017042-7 J. Geotech. Geoenviron. Eng.

J. Geotech. Geoenviron. Eng., 2017, 143(9): 04017042